Journal of Mechanical and Electrical Intelligent System (JMEIS)

A New Real-time Power Stabilization Method for WPT System

Hideo Kikuchi[1,a,*] , Ayana Nakajima[1,b] , Kazuhiro Motegi[1,c], and Yoichi Shiraishi[1,d]

[1] Graduate School of Science and Technology, Gunma University, 29-1 Ota-shi, Japan

*Corresponding author

[a]<kikuchih@y8.dion.ne.jp>, [b]<t182b005@gunma-u.ac.jp>, [c]<motegi@gunma-u.ac.jp>, [d]<yoichi.siraisi@gunma-u.ac.jp>

Keywords: wireless power transfer, coupling coefficients estimation, efficiency maximization of WPT, quality factor, adaptive mutual impedance compensation

Abstract. This paper proposes a new wireless power transfer system that stabilizes the power supply to the load of a mobile object whose position is not stable. This wireless power transfer system works by matching the frequencies of the AC power supply, the source coil resonator, the sending coil resonator, and the receiving coil resonator. In this system, all circuit impedances are always matched. The position of the source coil is moved to the optimum position so that the current from the power source remains constant. Then, the coupling coefficient between the source and sending coils is changed according to the coupling coefficient between the sending and receiving coils, and the power supply to the load circuit is stabilized.

1. Introduction

Magnetic resonant coupling is one of the most effective wireless power transfer (WPT) technology. The WPT system has a transmitter with a sending coil and a receiver with a receiving coil [1-13]. The design of the WPT system requires consideration of changes in alignment and in distance between these coils. The receiver in a moving object such as a helicopter easily changes distance from the transmitter [14, 15]. The magnitude of the received power decreases when the distance changes. Wireless power transfer efficiency (*PTE*) improves significantly by adjusting the distance between the source and sending coils according to the distance between the sending and receiving coils [4]. However, in that research, since the WPT system having a resonator whose resonant capacitance is the self-capacitance of the transmitting / receiving coil was studied, there was a problem that the shape of the coil was limited.

In this paper, we propose a new WPT system that can set the shape of the coils freely, and the WPT system compensates for the power supply to the load circuit according to the movement of the receiving coil L_3. It stabilizes the power supply to the load circuit of moving object whose position is not stable. To stabilize the power supply to the load circuit, the WPT system detects the current from the power supply and moves the position of the source coil according to the distance between the sending and receiving coils, which controls the mutual inductance (coupling coefficient) between the source and sending coils.

2. Real-time Power Adjusting Method

Figure 1 shows an experimental setup of the WPT system. In the WPT system, the source coil L_1 at the bottom of the figure is placed adjacent to the sending coil L_2. The source coil L_1 is 13-turn coil with a diameter of 20 cm. The source coil L_1 is placed off-axis from the axis of the sending coil L_2. The sending coil L_2, the receiving coil L_3, and the load coil L_4 is aligned in the coaxial direction. The load coil L_4 is a one-turn coil. This WPT system moves the source coil L_1 perpendicular to the coil axis

when the receiving coil L_3 moves. Moving the coil L_1 controls the coupling coefficient between the source coil L_1 and the sending coil L_2. It adapts to the movement of the receiving coil L_3 and compensates for the power supply to the load circuit, and greatly improves the wireless power transfer efficiency.

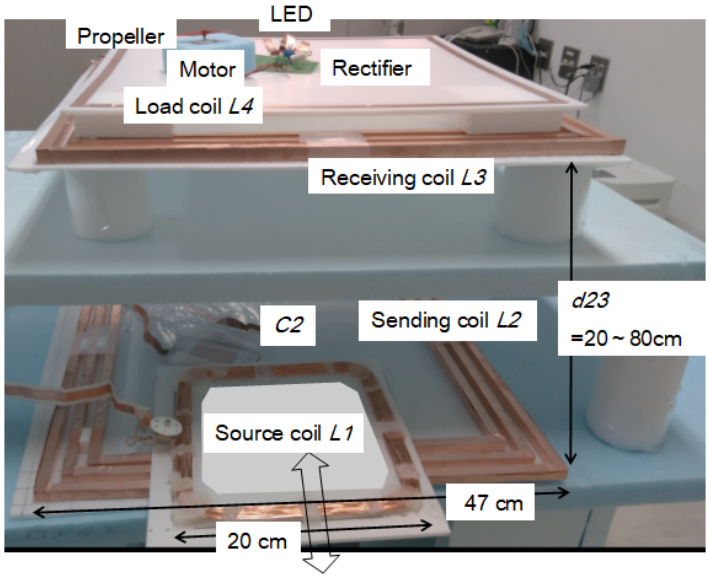

Fig. 1. Experimental setup.

2.1 WPT system configuration

Figure 2 shows the scheme of the experimental setup. Figure 3 shows the equivalent circuit of the WPT system. The WPT system has 2MHz resonators with a coil and a discrete capacitor. The resonators are a source coil resonator which has a source coil L_1 and a resonant capacitance C_1 and a power supply, a sending coil resonator which has a sending coil L_2 and a resonant capacitance C_2, a receiving coil resonator which has a receiving coil L_3 and a resonant capacitance C_3, a load coil resonator which has a load coil L_4 and a resonant capacitance C_4 and a load resistance R_4. The shape of the coils can be selected freely, and the capacitance of the discrete capacitor is selected accordingly.

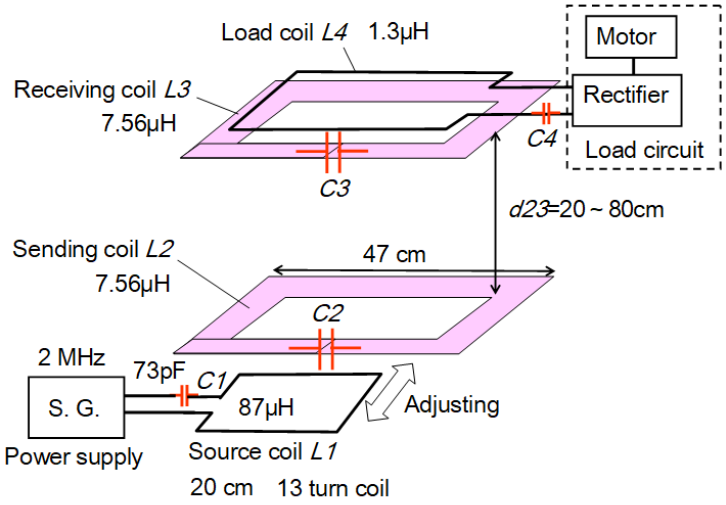

Fig. 2. Scheme of experimental setup.

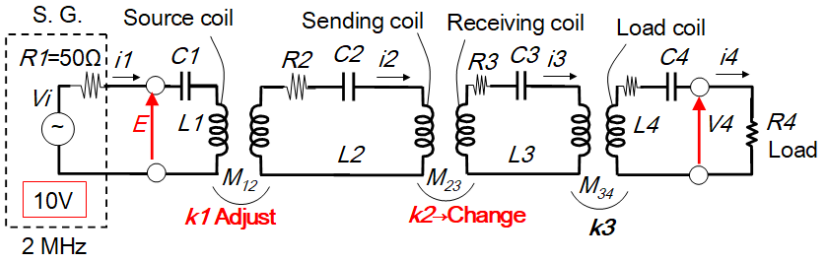

Fig. 3. Equivalent circuit.

In the equivalent circuit of Fig. 3, the load circuit which has a rectifier and an LED and a DC motor is simplified to one load resistance R_4. In the circuit, all circuit impedances are always matched at a frequency of 2 MHz. In this paper, the fixed angular frequency of $2\pi \times$ (2 MHz) is represented by ω.

The WPT system has an AC power supply S.G. with an output impedance of 50 Ω, a frequency of 2 MHz, and a constant voltage amplitude. The AC power supply S.G. is connected to the source coil. The source coil L_1 and the sending coil L_2 are inductively coupled to each other with a coupling coefficient of k_1. The sending coil L_2 and the receiving coil L_3 are inductively coupled to each other with a coupling coefficient of k_2. The coupling coefficient is the ratio of the mutual inductance between the coils to the self-inductance of the coils. The receiving coil L_3 and the load coil L_4 are inductively coupled to each other with a coupling coefficient of k_3.

The inductance of the sending coil L_2 and the receiving coil L_3 is 7.56 μH, respectively. The capacitance of C_2 and C_3 is 838 pF, respectively. The inductance of the source coil L_1 is 87 μH, and the load coil L_4 is 1.3 μH. The load resistance R_4 is 25 Ω. Resonant capacitance C_1 is 73 pF, C_4 is 4870 pF.

The electric power is transferred from the source coil L_1 to the load resistance R_4 via the coils L_2 and L_3 and L_4. Fig. 4 shows the coupling coefficient k_2 corresponding to the distance d_{23} between the coils L_2 and L_3.

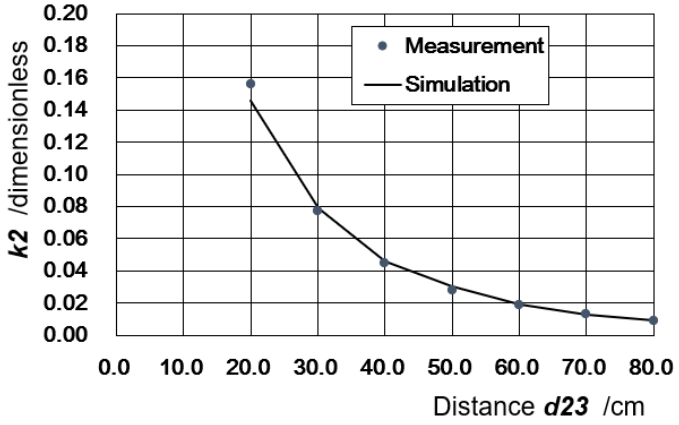

Fig. 4. Coupling coefficient k_2 between the coils L_2 and L_3.

The measured coupling coefficient k_2 and the simulation results are in good agreement. When the distance d_{23} between the coils L_2 and L_3 increases, the coupling coefficient k_2 decreases.

The source current i_1 supplied from the power supply S.G. is detected to control the circuit. The position of the source coil L_1 is moved so that the source current i_1 remains constant. Then, the coupling coefficient k_1 between the source coil L_1 and the sending coil L_2 is set according to the distance d_{23} between the coils L_2 and L_3 as shown in Fig. 23. And the coupling coefficient k_1 is set according to the coupling coefficient k_2 as shown in Fig. 24. By moving the sending coil L_1 in this way, the power supplied to the load resistance R_4 of the moving object is stabilized.

2.2 Shapes of the coils in the WPT system can be selected freely

In this WPT system, the shapes of the coils can be selected freely. In the WPT system, quality factors Q_2 of the sending coil resonator, quality factor Q_3 of the receiving coil resonator, and the coupling coefficient k_2 between coils L_2 and L_3 are the important factors that determine the power transfer efficiency of the WPT system. Replacing the sending coil L_2 or the receiving coil L_3 with a coil of a different inductance (with the resonant capacitance replaced) did not changed the performance of the WPT system.

Figure 5 shows another experimental setup of the WPT system. This experimental setup has 80 μH coils L_2 and L_3.

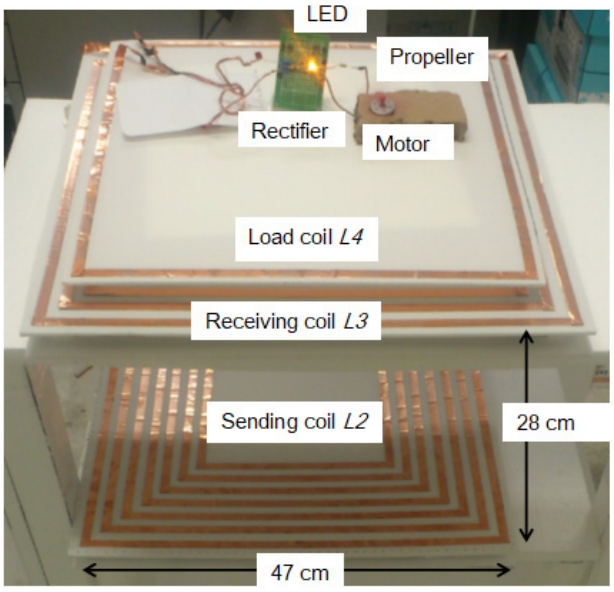

Fig. 5. Experimental setup. This WPT system works at 1.1 MHz. The inductance of L_2 and L_3 is 80 μH. They are double layer coils with 14 turns of flat conductor tape.

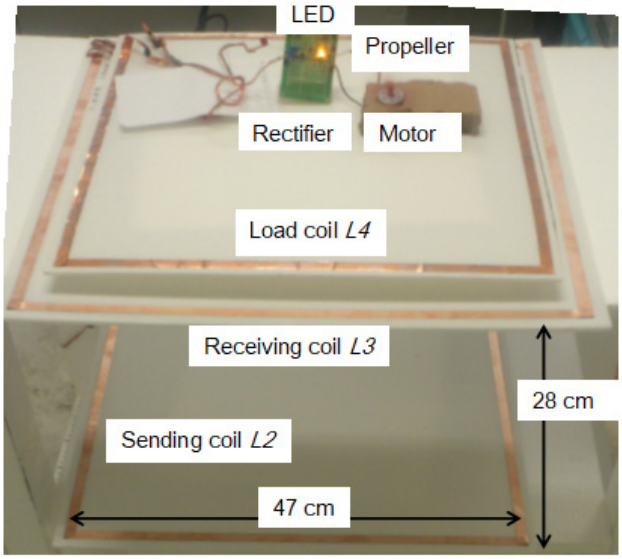

Fig. 6. Experimental setup. This WPT system works at 1.1 MHz. The inductance of L_2 and L_3 is 1.7 μH. They are 2-layer coils. They are coils with one turn of flat conductor tape.

Figure 6 shows yet another experimental setup of the WPT system. This experimental setup has 1.7μH coils L_2 and L_3.

Replacing the coils did not change the performance of the WPT system. Therefore, the quality factors Q_2 and Q_3 are more important than the shapes of the coils. And the coil shapes of this WPT system can be selected freely.

2.3 Sending coil L_2 and receiving coil L_3

Figure 7 shows the coil that was used for coils L_2 and L_3.

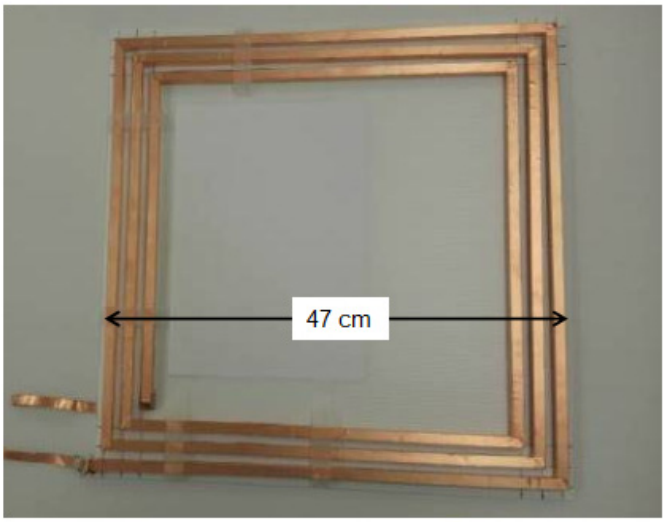

Fig. 7. Three-turn spiral coil. Inductance is 7.56 μH. AC resistance R_{ac} is 0.31 Ω. Quality factor is 313 at 2 MHz.

Three-turn spiral rod-coil with outer diameter of 47 cm was used for the sending coil L_2 and the receiving coil L_3. The 3-turn spiral rod-coil is a rod coil with a square cross section with a side of 1 cm. And on the surface of the rod coil, there is four parallel copper tape conductors with a thickness of 0.07 mm. The volume resistivity of the copper tape was 1.42 times the resistivity of pure copper. The inductance of the coil is 7.56 μH. The self-resonant frequency of the coil is 11 MHz and the self-capacitance of the coil is 18 pF. The externally added lumped capacitance (resonant capacitance C_2 or C_3 minus self-capacitance) is 820 pF.

The coupling coefficient k_2 between the coils L_2 and L_3 corresponding to the distance between them are shown in Fig. 4. When the distance between the coils L_2 and L_3 is about 47 cm that is same as the diameter of these coils, the coupling coefficient k_2 between the coils is about 0.03.

2.3.1 Q-factor measurement of the coils L_2 and L_3

The quality factor (Q factor) Q_2 of the sending coil resonator and Q_3 of the receiving coil resonator were almost the same as the quality factor of these coils. The quality factor of these coils is influenced by the coil size and resonant frequency. To increase wireless power transfer efficiency (*PTE*), the quality factor of the resonant coils must be high.

A 2 MHz resonator was constructed using this coil and a high-Q lumped resonant capacitor with a capacitance of 820 pF. We made a high-Q PTFE film capacitor for the experiment. The measured quality factor of the resonator at 2 MHz was 313. The quality factor of the coil is inversely proportional to the AC resistance R_{ac} of the coil. The measured AC resistance R_{ac} of the coil was 0.31 Ω. The AC

resistance R_{ac} is about 4.4 times the 0.071 Ω AC resistance of a straight rod wire with the same length and surface area as this coil. This ratio 4.4 is AC resistance ratio of the coil.

2.3.2 Proximity effect factor of the coil

One of the causes of this AC resistance ratio 4.4 is thought to be the proximity effect [16]. R.G. Medhurst has provided data on the AC resistance of coils based on numerous experiments in 1947 [16]. Table 1 shows a part of Table 8 in Medhurst's report.

Table 1. Proximity Effect Factors (Ψ) of Coils.

Wire d/pitch	(Coil Length h)/(Coil Diameter D)					
	0.0	0.2	0.4		10.0	∞
1.0	5.31	5.45	5.65		3.23	3.41
0.9	3.73	3.84	3.99		2.93	3.11
0.8	2.74	2.83	2.97		2.65	2.815
0.7	2.12	2.2	2.28		2.27	2.51
0.6	1.74	1.77	1.83		2.1	2.22
0.5	1.44	1.48	1.54		1.83	1.93
0.1	1.02	1.02	1.03		1.04	1.05

Table 1 shows proximity effect factors (Ψ) based on the geometrical characteristics of the coil. Proximity effect factor (Ψ) is the ratio of the AC resistance of the coil to that of a straight wire of the same length and surface area. Figure 8(a) shows the wire diameter d and wire pitch. The left column of the Table 1 shows the (wire diameter *d*) / (wire pitch) parameters of the coil.

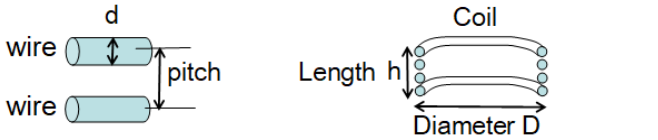

(a) Wire pitch (b) Coil length h and coil diameter *D*

Fig. 8. Proximity Effect Factors (Ψ) of Coils.

The proximity effect factor (Ψ) in the lower column of Table 1 shows the proximity effect factor (Ψ) of a coil with sparsely arranged parallel wires. Fig. 8(b) shows the coil length h and coil diameter D. The top column of the Table 1 shows the (coil length h) / (coil diameter D) parameters of the coil. Medhurst has examined coils with 30-50 turns, so the information that Medhurst data shows is limited to coils with many windings.

In the following, we will consider the table data corresponding to the measurement results for a 2 cm wide tape coil. The data corresponding to the coil is the data on the left side of Table 1 showing the coil with a small (length h)/(diameter). The 2 cm wide tape-like coil is equivalent to a coil with closely spaced wires at the top of Table 1. Therefore, 5.31 and 5.45 in Table 1 can be used as the data corresponding to the equivalent coil bundle of the tape-like coil.

The surface area of a tape-like conductor is (2/π) times the surface area of the equivalent coil bundle. The surface area of a straight circular cross-section wire with the same length and surface area as this tape-like conductor is (2/π) times the surface area of the equivalent coil bundle. The AC resistance of the straight circular cross-section wire is (π/2) times the AC resistance of the straight circular cross-section wire of the same length and surface area as the equivalent coil bundle. Therefore, the ratio of the AC resistance of the tape-like conductor coil to the AC resistance of a straight circular cross-section

wire with the same surface area as this tape-like coil is (2/π) times the data 5.31-5.45. This is 3.4-3.5. The measured AC resistance ratio 4.4 is larger than this ratio.

2.3.3 AC resistance obtained by simulation

The AC resistance of the coil was calculated by simulation [6-13]. The AC resistance R_{ac} of the spiral rod coil was obtained by simulation using the 3D electromagnetic field simulation software FastHenry [17, 18], which calculates the AC resistance R_{ac} and inductance of the coil.

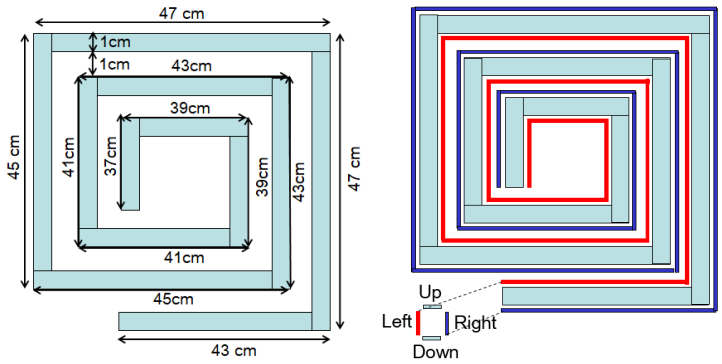

(a) Plan view of the coil model. (b) Layout of 4 copper tapes.

Fig. 9. Layout of 4 copper tapes in the coil.

Figure 9 shows the spiral rod coil of the simulation model. The model uses a spiral rod coil with four parallel copper tape conductors with a thickness of 0.035 mm on the surface. The thickness of 0.035 mm of the tape is thinner than the depth of the copper skin effect at 2 MHz. Since the volume resistivity of the copper tape was 1.42 times the resistivity of pure copper, the depth of the copper skin effect is 0.056 mm at 2 MHz. The simulation gave an AC resistance of 0.34 Ω. This value is close to the measured AC resistance.

Next, as shown in Fig. 10, the coil model was changed to a model in which four parallel copper tapes were connected at the bending points of the coil.

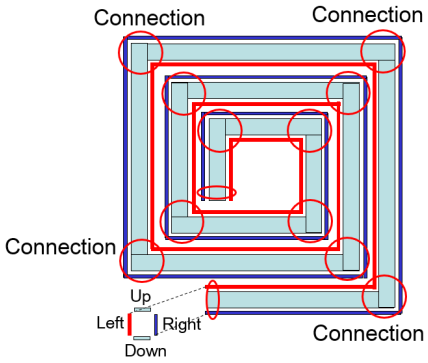

Fig. 10. Connection point of cupper tape in the simulation.

The AC resistance of the coil obtained in the simulation has decreased from 0.34 Ω obtained in the previous simulation to 0.24 Ω.

To experimentally confirm the effect of the copper tape connection, the copper tape on the right side and the copper tape on the left side of the spiral rod coil were connected at two bending points as shown in Fig. 11.

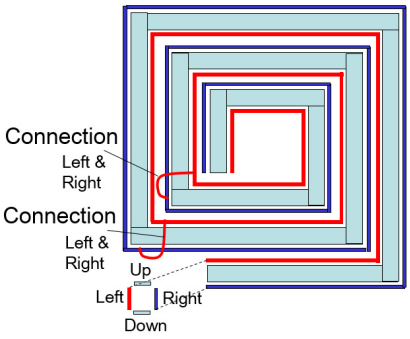

Fig. 11. Connection point of copper tape in the experiment.

The measured AC resistance of the coil has dropped from the previous measurement of 0.31 Ω to 0.26 Ω. This is thought to be because the AC resistance of each part of the coil is different.

Figure 12 shows the AC resistance R_{ac} of the coil as a function of the frequency given by the simulation. FastHenry simulates the characteristics of a coil with a negligible displacement current [18], so the simulation results at frequencies lower than the coil's self-resonant frequency of 11 MHz are valid.

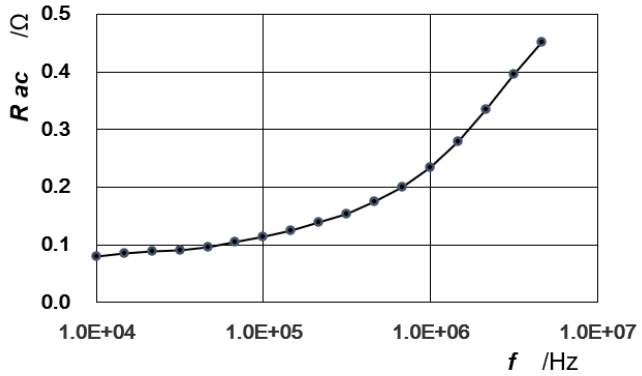

Fig. 12. AC resistance R_{ac} of the coil as a function of the frequency.

The AC resistance R_{ac} of the coil increases with frequency. The thickness of 0.035 mm copper tape is thinner than the depth of the skin effect of copper, so its AC resistance is unaffected by the skin effect. The phenomenon of increase in the AC resistance of the coil due to frequency is thought to be due to the phenomenon that the difference in current density depending on the position of the coil increases with frequency.

2.3.4 Further improvement of coil Q-factor

In Table 1, the proximity effect factor (Ψ) or AC resistance R_{ac} is reduced for coils with sparsely arranged parallel lines. This means the quality factor will be higher if the coil wires are sparsely arranged. A high-quality-factor coil with sparsely arranged parallel wires has been reported [8, 12].

To confirm the effect of the sparsely arranged wires, the following two coils were prepared, measured the quality factor, and compared them. Figure 13 shows the two coils.

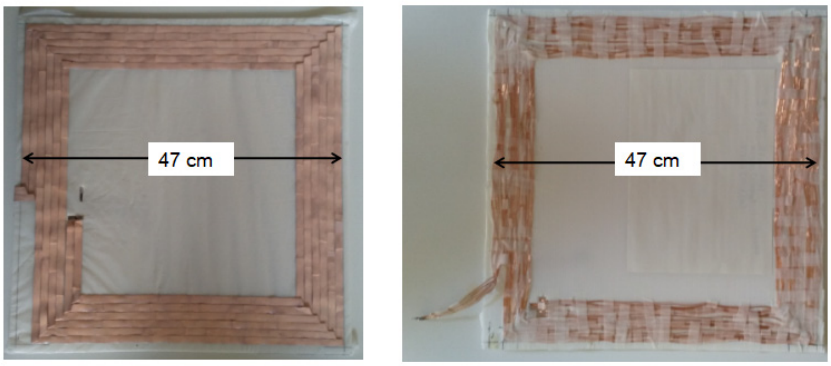

(a) Conductor tape coil.
L : 7.0μH
C : 907pF
AC resistance : 0.63Ω
Quality factor : 139 at 2MHz

(b) Sparse wire bundle coil.
L : 8.12μH
C : 795pF
AC resistance : 0.37Ω
Quality factor : 275 at 2MHz

Fig. 13. Three-turn spiral flat coil.

Figure 13(a) shows a 3-turn spiral flat coil with conductor tape. it is a flat coil in which a conductor tape with a width of 2 cm and a thickness of 0.14 mm is wound three times without any gaps. Figure 13(b) shows a 3-turn spiral flat coil with sparse wire bundle. it is a 3-turn flat coil formed by winding a flat wire bundle with a width of 2 cm. The flat wire bundle is a bundle of wires with a diameter of 0.2 mm arranged in a width of 2 cm with a gap of 0.2 mm. The measured quality factor of the coil with conductor tape was 139 at 2 MHz. The measured quality factor of the coil with sparse wire bundle was 275 at 2 MHz. The quality factor of the coil with sparse wire bundle was twice that of the coil with conductor tape.

3. Theory and numerical simulation

The electrical performance of the circuit of the WPT system is calculated by the filter theory [3]. And the voltage-current equation of the circuit has been solved [5]. Fig. 14 shows a circuit for a WPT system simulation. Figure 15 show the results of the simulation.

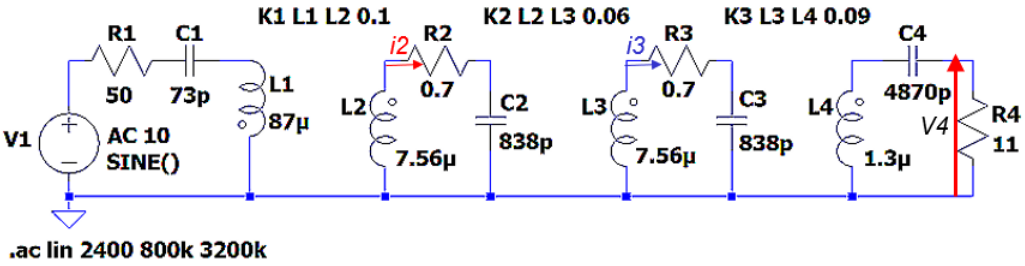

Fig. 14. A circuit for a WPT system simulation.

Figure 15 has a graph as a function of the frequency of the current i_2 of the sending coil L_2, the current i_3 of the receiving coil L_3, and the load voltage V_4 applied to the load resistance R_4. In the graph of the voltage V_4 on the load resistance R_4, three resonant frequencies f_1, f_2, and f_3 are observed. In the graph of the current i_2 of the sending coil L_2, only two resonant frequencies f_1 and f_3 are observed. We used the 2 MHz resonant frequency in the middle of the three resonant frequencies.

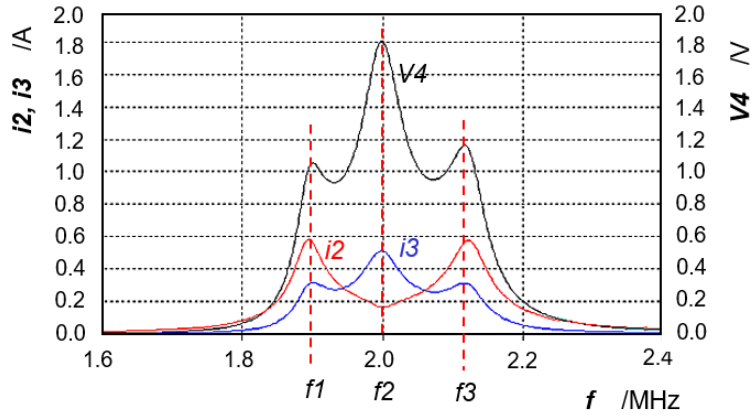

Fig. 15. Results of the WPT system simulation.

3.1 Formula of ratio between currents and formula of image impedance

In the equations, the fixed angular frequency of 2π × (2MHz) is represented by ω. The current ratio and image impedance of the equivalent circuit in Fig. 3 are derived as follows:

$$\frac{i_2}{i_1} = \frac{j\omega L_4}{R_4}\sqrt{\frac{L_1}{L_2}}k_1\left(\frac{k_3}{k_2}\right)^2 , \tag{1}$$

where, ω is the fixed resonant angular frequency 2π × (2 MHz), $i_1 = |i_1|(\cos(\omega t)+i\sin(\omega t))$.

$$\frac{i_3}{i_1} = -\sqrt{\frac{L_1}{L_3}}\frac{k_1}{k_2} , \tag{2}$$

$$\frac{V_4}{R_4} = i_4 = \frac{-j\omega\sqrt{L_1L_4}}{R_4}(s)i_1 , \tag{3}$$

where,

$$s = \left(\frac{k_1k_3}{k_2}\right), \tag{3b}$$

Calculating the input voltage E that is generated in coil L_1 by electromagnetic induction between the coils L_1 and L_2 yields image impedance Eq. (4).

$$Z_{in} = \frac{E}{i_1} = \frac{\omega^2 L_1L_4}{R_4}(s)^2 , \tag{4}$$

Equation (4) of image impedance Z_{in} is expressed by L_1 and L_4, and there is no effect of L_2 or L_3. This means that the image impedance Z_{in} does not change even if the sending coil L_2 or the receiving coil L_3 are replaced to the coils of different inductances (with the resonant capacitance replaced).

The source current i_1 is derived using the image impedance Z_{in} as follows.

$$i_1 = \frac{V_i}{R_1 + Z_{in}} = \frac{V_i}{R_1 + \frac{\omega^2 L_1L_4}{R_4}(s)^2} , \tag{5}$$

Equation (5) represents the source current i_1 as a function of parameter s. By substituting Eq. (5) into Eq. (3), it yields Eq. (6).

$$V_4 = \frac{jV_i}{\frac{R_1}{s\omega\sqrt{L_1L_4}} + \frac{s\omega\sqrt{L_1L_4}}{R_4}}, \tag{6}$$

Equation (6) represents the load voltage V_4 as a function of parameter s. Parameter s is a function of the coupling coefficient k_1 as shown in Eq. (3b).

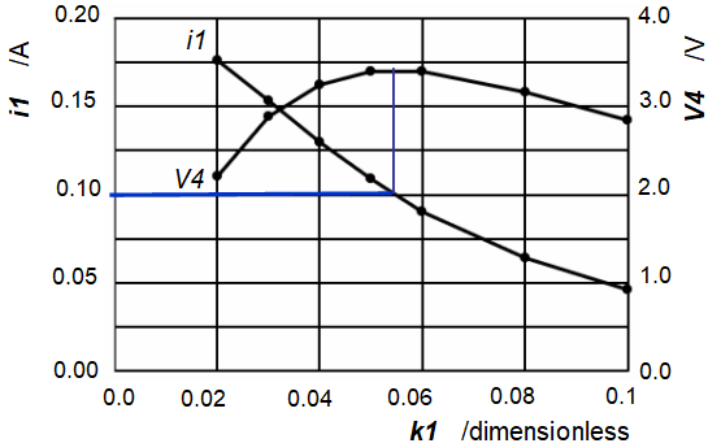

Fig. 16. Source current i_1 and Load voltage V_4. The coupling coefficient k_2 is 0.06.

Figure 16 shows a graph of the circuit simulation results for source current i_1 and load voltage V_4 corresponding to the coupling coefficient k_1. The parameter s is a function of the coupling coefficient k_1. The simulation results matched theoretical equations. In the theoretical equations Eq. (4) to (6), when the parameter s is kept constant, image impedance Z_{in} and source current i_1 and V_4 are kept constant. To keep the parameter s constant, the source coil L_1 is moved to keep the amplitude of the source current i_1 constant.

When the relative position between the source coil L_1 and the sending coil L_2 is at the optimum position, the load voltage V_4 becomes maximum. When the parameter s is kept constant by making k_1 proportional to k_2, the image impedance Z_{in} will be constant. In that case, the amplitudes of source current i_1 and E will be constant in proportion to V_i. To keep V_4 constant, the position of L_1 is adjusted so that the amplitude of i_1 is constant.

3.2 Coupling coefficient k_1 between the coils L_1 and L_2 obtained by simulation

Figure 17 shows an electromagnetic field simulation model and the coupling coefficient k_1 between the source coil L_1 and the sending coil L_2. In the figure, X is the horizontal shift length of the source coil L_1.

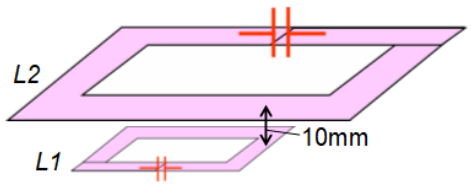

(a) Perspective view of coils L_1 and L_2

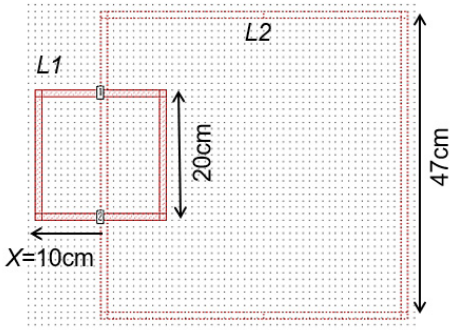

(b) Top view of coils L_1 and L_2. The horizontal shift length X of the source coil L_1 is 10 cm. The coupling coefficient k_1 is 0.03.

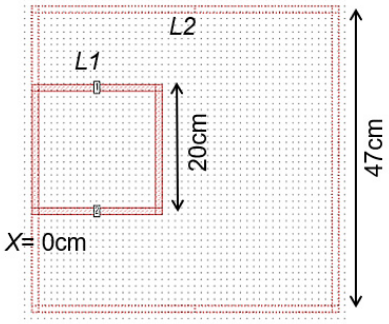

(c) Top view of coils L_1 and L_2. The horizontal shift length X of the source coil L_1 is 0 cm. The coupling coefficient k_1 is 0.16.

Fig. 17. Simulation model and coupling coefficient k_1.

Figure 18 shows electromagnetic field simulation results of the coupling coefficient k_1 between the source coil L_1 and the sending coil L_2 corresponding to the horizontal shift length X of the source coil L_1.

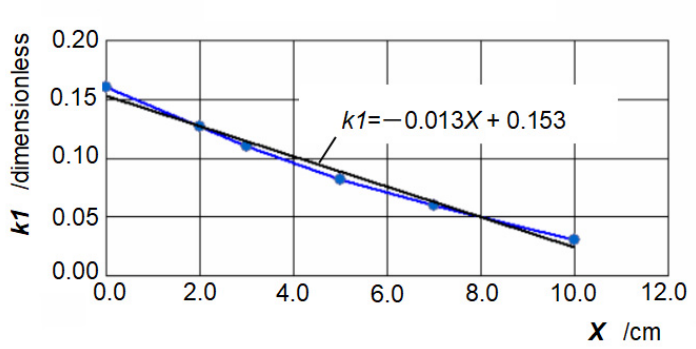

Fig. 18. Coupling coefficient k_1 vs. horizontal shift length X.

Equation (7) is an approximate equation of the coupling coefficient k_1 corresponding to the horizontal shift length X.

$$k_1 = -0.013x[cm] + 0.153, \tag{7}$$

3.3 Wireless power transfer efficiency of the WPT system

The wireless power transfer efficiency (*PTE*) of the WPT system is calculated as follows:

$$PTE=\frac{R_4|i_4|^2}{\left(R_2|i_2|^2+R_3|i_3|^2+R_4|i_4|^2\right)}=\left(\frac{P}{k_2Q_2}+\frac{1}{k_2Q_3P}+1\right)^{-1}, \tag{8}$$

where,

$$P=\frac{\omega L_4 k_3^{\,2}}{R_4 k_2}, \tag{8b}$$

PTE depends on the coupling coefficient k_2 between the coils L_2 and L_3 and the quality factors Q_2 of the sending coil resonator and Q_3 of the receiving coil resonator. Q_2 and Q_3 are inversely proportional to the losses of the resonators, which is the sum of the coil loss and the capacitor loss. It is desirable to set the coupling coefficient k_2 and k_3 and the inductance L_4 so that the parameter P is approximately equal to 1.

3.4 Effects of Coupling Coefficients between Non-adjacent Coils

Figure 19 shows the coupling coefficient between non-adjacent coils in the equivalent circuit of the WPT system.

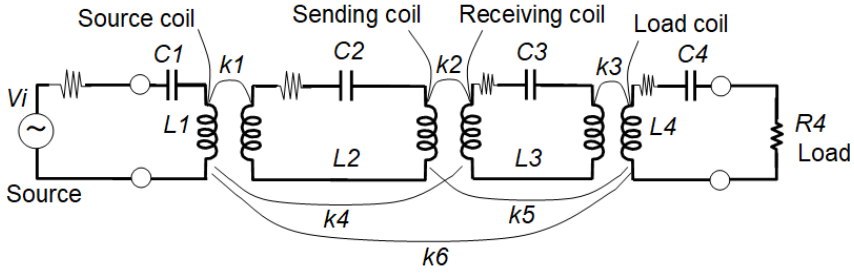

Fig. 19. Coupling coefficient between non-adjacent coils.

The equations for the effects of the coupling coefficients between the non-adjacent coils of the equivalent circuit in Fig. 19 are derived as follows:

$$Z_{in}=\frac{E}{i_1}=\frac{\omega^2 L_1 L_4}{R_4}(s)^2\left(1+\frac{2jk_4}{Pk_1}\right), \tag{9}$$

$$\frac{i_1}{i_4}=\frac{-R_4}{j\omega\sqrt{L_1L_4}}\left(\frac{1}{s}\right)\left(1+2jP\frac{k_5}{k_3}\right), \tag{10}$$

$$Z_{in}=\frac{E}{i_1}=\frac{\omega^2 L_1 L_4}{R_4}(s)^2\left(1-\frac{k_2k_6}{k_1k_3}\right)^2, \tag{11}$$

The non-adjacent coupling coefficients can be obtained by electromagnetic field simulation. k_4 is about 1/3 of k_2. k_6 is less than k_4. k_5 is approximately equal to k_2. As shown in Eq. (9), the non-adjacent coupling coefficient k_4 effects on image impedance Z_{in}. As shown in Eq. (10), the non-adjacent coupling coefficient k_5 effects on the current ratio i_1 / i_4. As shown in Eq. (11), the non-adjacent coupling coefficient k_6 effects on image impedance Z_{in}.

The effects of non-adjacent coupling coefficients are simulated in Simulation 2 in Chapter 4.

4. Experimental results

4.1 Experimental setup with axial shift of the source coil

One experiment was conducted to measure the characteristics of the WPT system. Fig. 20 shows the experimental setup.

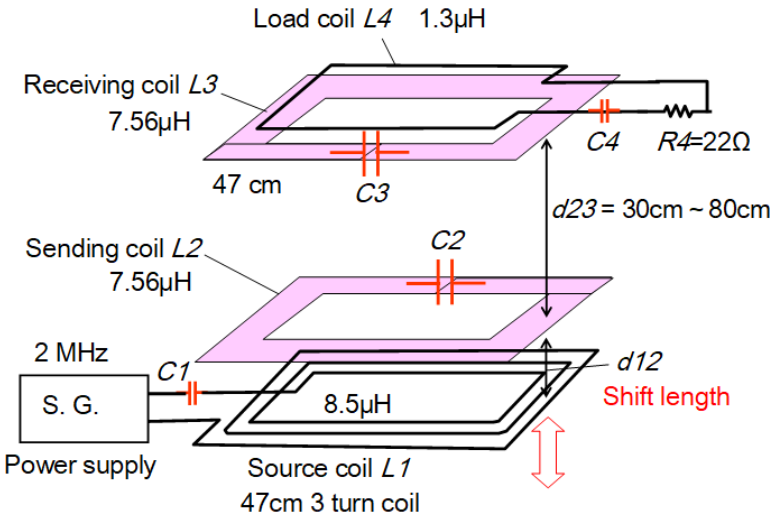

Fig. 20. Scheme of experimental setup.

For the source coil L_1, a 3-turn flat conductor tape spiral coil with a tape width of 1 cm and an outer diameter of 47 cm was used. A resonant capacitance C_1 and a power supply S.G. were connected to the source coil L_1. For the sending coil L_2 and the receiving coil L_3, 3-turn spiral rod-coil with outer diameter of 47 cm was used. A variable capacitor C_2 and C_3 were used for the resonant capacitance of the sending coil resonator and the receiving coil resonator. Resonant frequency of these resonators can be easily adjusted with the variable capacitor. The resistance of the sliding contacts in the variable capacitor was added to the series resistance of the resonator. For the load coil L_4, a flat 1-turn coil with outer diameter of 36 cm was used. A resonant capacitance C_4 and the load resistance R_4 were connected to the load coil L_4.

The load resistance R_4 is 22 Ω. The inductance of the load coil L_4 is 1.3 μH and C_4 is 4870 pF. The distance between L_3 and L_4 is 7 cm. The coupling coefficient k_3 between L_3 and L_4 is 0.26. The inductance of the sending coil L_2 and the receiving coil L_3 is 7.56 μH, respectively. The capacitance of C_2 and C_3 is 838 pF, respectively. The inductance of the source coil L_1 is 8.5 μH. Resonant capacitance C_1 is 744 pF.

The currents in the sending coil resonator and the receiving coil resonator were detected by the current sensor installed in each coil. The current sensor is made up of a current detection coil and a sensing rectifier. The current detection coil is an air-core coil with a diameter of 48 mm. The coil has one turn of the primary coil and 4 turns of the secondary coil. In the current sensor, the secondary coil is connected to the sensing rectifier. The resonator current is measured by the rectified DC voltage of the sensing rectifier. The current sensor added a series resistance of 0.08 Ω to the resonator. The total series resistance of each resonator was 0.58 Ω and 0.68 Ω, respectively. The source current i_1 was measured by another current sensor.

The distance d_{23} between the coils L_2 and L_3 varied from 20 to 80 cm, in 10 cm steps. When the distance d_{23} between the coils L_2 and L_3 increases, the coupling coefficient k_2 decreases. To keep the amplitude of the source current i_1 constant at 0.9 A, the source coil L_1 was moved parallel to the coil

axis according to the distance d_{23} between L_2 and L_3. When the source current i_1 was kept constant, the load voltage V_4 applied to the load resistance R_4 was stabilized.

Figure 21 shows the measured power transfer efficiency (*PTE*) when the load resistance R_4 is 22 Ω. The power output from the AC power supply S.G. is defined as a constant value of the product of 0.9A and 4.8 V, and the ratio of the power consumed by the load resistance R_4 to that power is defined as *PTE*. The solid line shows the first simulation results. The broken line shows the results of Simulation 2. In Simulation 2, the coupling coefficient between non-adjacent coils are included in the calculation.

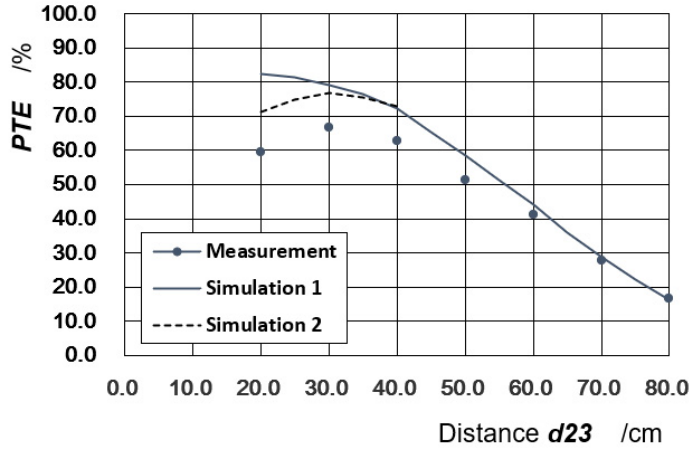

Fig. 21. Power transfer efficiency of the WPT system.

4.2 Experimental setup with horizontal shift of the source coil

Another experiment was conducted to measure the characteristics of the WPT system. Figure 22 shows the experimental setup. The same coils as in the experiment in Section 4.1 were used. In the experiment, the source coil L_1 was moved perpendicular to the coil axis according to the distance d_{23} between the coils L_2 and L_3 in order to keep the amplitude of the source current i_1 constant at 0.9 A.

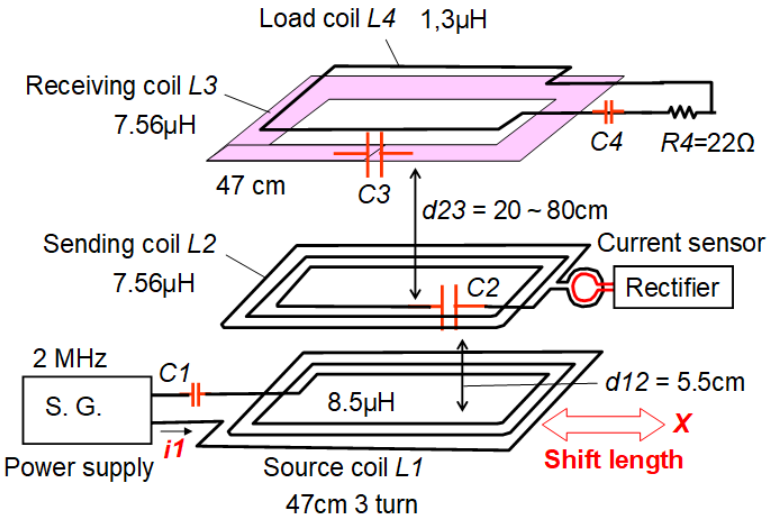

Fig. 22. Scheme of experimental setup.

Figure 23 shows the horizontal shift length X of the source coil L_1 according to the distance d_{23} between the coils L_2 and L_3 of the experiment. k_1 is the coupling coefficient between the coils L_1 and L_2.

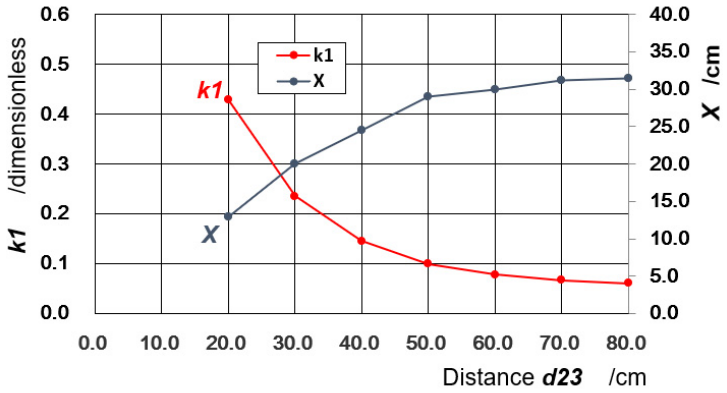

Fig. 23. Coupling coefficient k_1 and the horizontal shift length X.

Figure 24 shows the coupling coefficient k_1, k_2, and the parameter s. The parameter s is the ratio between them, which is shown in Eq. (3b).

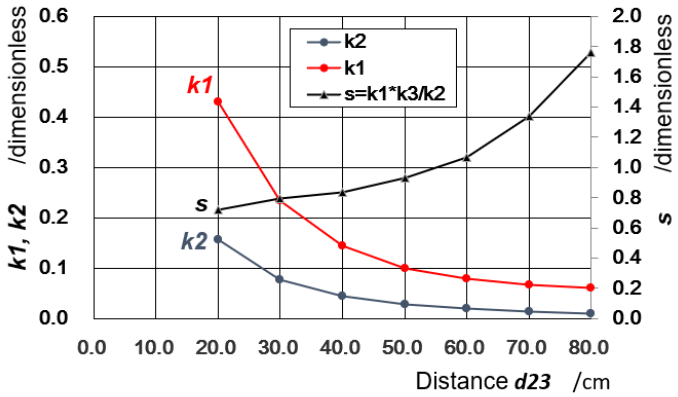

Fig. 24. Coupling coefficient k_1, k_2, and the parameter s.

In the experiment, the parameter s changed according to the distance d_{23} between the coils L_2 and L_3. The reason the parameter s was not kept constant is due to the resonator loss in the WPT system.

Figure 25 shows the measured input voltage E applied to the source coil L_1. The solid line shows simulation results. The broken line shows the results of Simulation 2. In Simulation 2, the coupling coefficient between non-adjacent coils are included in the calculation. The input voltage E was 4.8 V except when the distance d_{23} between the coils L_2 and L_3 was 20 cm.

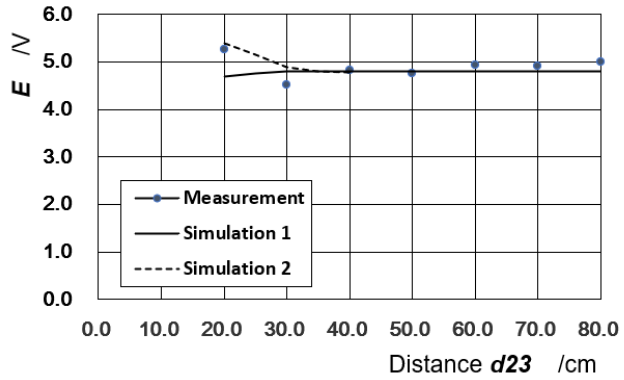

Fig. 25. Input voltage *E* applied to the source coil L_1.

Figure 26 shows the measured current i_2 in the sending coil L_2.

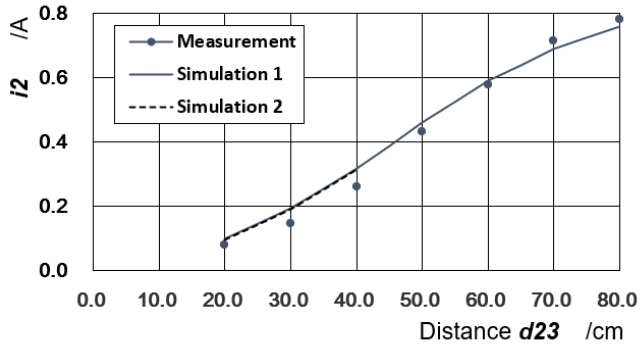

Fig. 26. Current i_2 in the sending coil L_2.

Figure 27 shows the measured current i_3 in the receiving coil L_3.

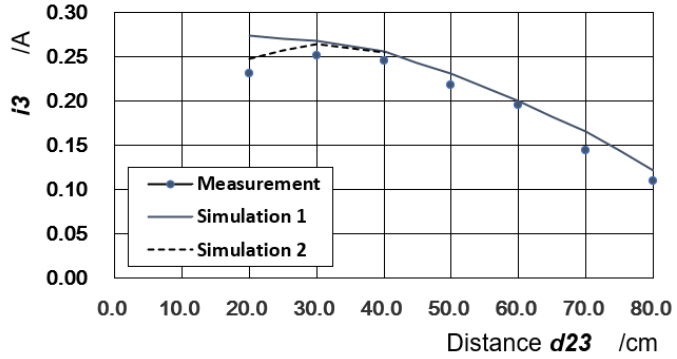

Fig. 27. Current i_3 in the receiving coil L_3.

Figure 28 shows the load voltage V_4 applied to the load resistance R_4.

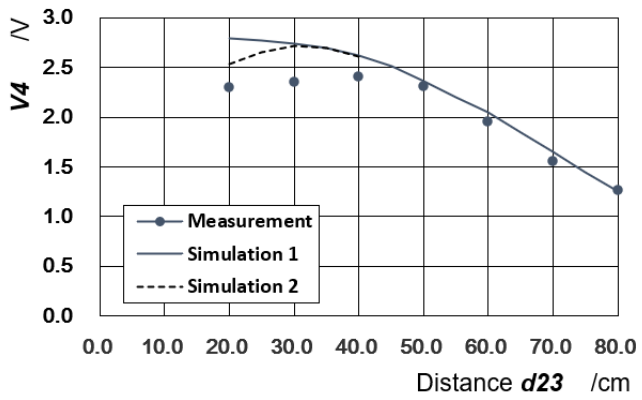

Fig. 28. Load voltage V_4 applied to the load resistance R_4.

Figure 29 shows the measured power transfer efficiency (*PTE*) of the experiment. The power output from the AC power supply S.G. is defined as a constant value of the product of 0.9 A and 4.8 V, and the ratio of the power consumed by the load resistance R_4 to that power is defined as *PTE*.

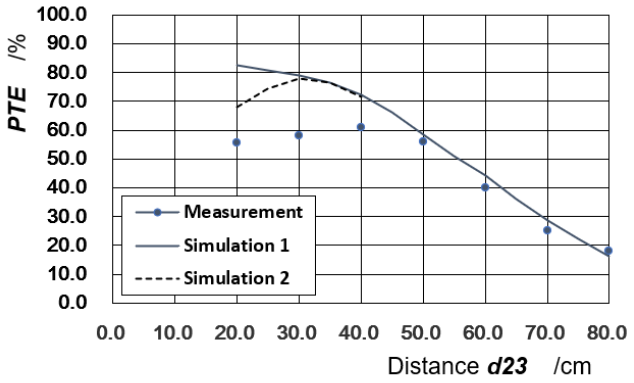

Fig. 29. Power transfer efficiency of the WPT system.

The measurement results and the simulation results were almost in agreement. The coupling coefficient between non-adjacent coils broke impedance matching, therefore the wireless power transfer efficiency decreased when the distance between coils L_2 and L_3 is small. The power supplied to the load resistance R_4 of the moving object was kept constant when the distance d_{23} between the sending coil L_2 and the receiving coil L_3 is between 20 cm and 50 cm.

5. Conclusions

The wireless power transfer at the middle resonant frequency of the three resonant frequencies was investigated. The WPT system moves the source coil L_1 perpendicular to the coil axis as the receiving coil L_3 moves. This stabilized power transfer to the load. The AC resistance of the coil increased due to the proximity effect. The proximity effect reduced the quality factor of the coils and reduced the efficiency of wireless power transfer of the WPT system. The quality factor of the coil can be improved by forming the coil with sparsely arranged wires. The coupling coefficient between non-adjacent coils breaks impedance matching of the circuit when the distance d_{23} between coils L_2 and L_3 is small. That decreased the wireless power transfer efficiency.

References

[1] A. Kurs, A. Karalis, R. Moffatt, J. D. Joannopoulos, P. Fisher and M. Soljačić, "Wireless power transfer via strongly coupled magnetic resonances", ***SCIENCE***, Vol. 317, pp. 83-86, 2007.

[2] T. Imura, H. Okabe and Y. Hori, "Basic Experimental Study on Helical Antenna of Wireless Power Transfer for Electric Vehicles by using Magnetic Resonance Couplings", ***IEEE Vehicle Power and Propulsion Conference*** (Dearborn, MI, USA), pp.936-940. September 2009.

[3] T. Ishizaki, T. Komori, T. Ishida and I. Awai, "Comparative study of coil resonators for wireless power transfer system in terms of transfer loss", ***IEICE Electronics Express***, Vol. 7, No. 11, pp. 785-790, 2010.

[4] T. P. Duong and J.-W. Lee, "Experimental results of high-efficiency resonant coupling wireless power transfer using a variable coupling method", ***IEEE Microwave and Wireless Component Letters***, Vol. 21, No. 8, pp. 442-444, 2011.

[5] C.K. Lee, W.X. Zhong and S.Y.R. Hui, "Effects of magnetic coupling of nonadjacent resonators on wireless power domino-resonator systems", ***IEEE Transactions on Power Electronics***, Vol. 27, No. 4, pp. 1905-1916, 2012.

[6] S.-H. Lee and R.D. Lorenz, "Surface Spiral Coil Design Methodologies for High Efficiency High Power Low Flux Density Large Air-Gap Wireless Power Transfer Systems", ***Applied Power Electronics Conference and Exposition (APEC) 2013 IEEE*** (Long Beach, CA, USA), pp. 1783-1790, March 2013.

[7] B.H. Waters, B.J. Mahoney, G. Lee and J. R. Smith, "Optimal coil size ratios for wireless power transfer applications", ***International Symposium on Circuits and Systems (ISCAS) 2014 IEEE*** (Melbourne VIC, Australia), pp. 2045-2048, June 2014.

[8] J.P.K. Sampath, A. Alphones, D.M. Vilathgamuwa, A. Ong and X. B. Nguyen, "Coil enhancements for high efficiency wireless power transfer applications", ***Industrial Electronics Society IECON 2014 - 40th Annual Conference of the IEEE*** (Dallas, TX, USA), pp. 2978-2983, October 2014.

[9] C. Kainan and Z. Zhengming, "Analysis of the Double-Layer Printed Spiral Coil for Wireless Power Transfer", ***IEEE Journal***, Vol. 1, pp. 114-121, 2013.

[10] C. Yang and K. Tsunekawa, "A novel parallel double-layer spiral coil for coupled magnetic resonance wireless power transfer", ***Wireless Power Transfer Conference (WPTC) 2015 IEEE*** (Boulder, CO, USA), May 2015.

[11] Y. Kawase, T. Yamagichi, D. Kato, S. Tsukada, K. Ito, K. Ida, Y. Fukui and N. Nishikawa, "Numerical analysis of stranded wire coil with magnetic substrate using 3-D finite element method", ***International Conference on Electrical Machines and Systems*** (Pattaya, Thailand), pp.985-988, October 2015.

[12] G. Zhu and R. D. Lorenz, "Achieving Low Magnetic Flux Density and Low Electric Field Intensity for a Loosely Coupled Inductive Wireless Power Transfer System", ***IEEE Transactions on Industry Applications***, Vol. 54, No. 6, pp. 6383 – 6393, 2018.

[13] G. Qian, Y. Cheng, G. Chen and G. Wang, "New AC resistance calculation of printed spiral coils for wireless power transfer", ***2018 19th International Symposium on Quality Electronic Design (ISQED)*** (Santa Clara, CA, USA), pp. 286-289, March 2018.

[14] G. M. Plaizier, E. Andersen, B. Truong, X. He, S. Roundy and K.K. Leang, "Design, Modeling, and Analysis of Inductive Resonant Coupling Wireless Power Transfer for Micro Aerial Vehicles

(MAVs)", ***International Conference on Robotics and Automation (ICRA) 2018 IEEE*** (Brisbane, QLD, Australia), pp. 6104-6109, May 2018,

[15] T. Campi, S. Cruciani and M. Feliziani, "Wireless Power Transfer Technology Applied to an Autonomous Electric UAV with a Small Secondary Coil", ***Energies***, Vol. 11, No. 2, pp. 352, 2018.

[16] R.G. Medhurst, "H.F. resistance and self-capacitance of single-layer solenoids – Part2", ***Wireless Eng.***, Vol. 24, pp. 80–92, March 1947.

[17] The 3D electromagnetic field simulation software FastHenry: http://www.fastfieldsolvers.com/

[18] M. Kamon, M.J. Tsuk and J.K. White, "FASTHENRY: a multipole-accelerated 3-d inductance extraction program", ***IEEE Trans. on Microwave Theory and Techniques***, Vol. 42, No. 9, pp. 1750–1758, 1994.